

Effect of hidden geometry and higher-order interactions on the synchronization and hysteresis behaviour of phase oscillators on 5-cliques simplicial assemblies

Samir Sahoo^{2,5}, Bosiljka Tadić^{1,4}, Malayaja Chutani³ and Neelima Gupte^{3,5}

¹*Department of Theoretical Physics, Jožef Stefan Institute, Jamova 39, Ljubljana, Slovenia*

²*Department of Applied Mechanics, Indian Institute of Technology Madras, Chennai 600036, India*

³*Department of Physics, Indian Institute of Technology Madras, Chennai 600036, India*

⁴*Complexity Science Hub, Josephstaedterstrasse 39, Vienna, Austria and*

⁵*Center for Complex Systems & Dynamics, Indian Institute of Technology Madras, Chennai 600036, India*

(Dated: May 25, 2023)

The hidden geometry of simplicial complexes can influence the collective dynamics of nodes in different ways depending on the simplex-based interactions of various orders and competition between local and global structural features. We study a system of phase oscillators attached to nodes of 4-dimensional simplicial complexes and interacting via positive/negative edges-based pairwise K_1 and triangle-based triple $K_2 \geq 0$ couplings. Three prototypical simplicial complexes are grown by aggregation of 5-cliques, controlled by the chemical affinity parameter v , resulting in sparse, mixed, and compact architecture, all of which have 1-hyperbolic graphs but different spectral dimensions. By changing the interaction strength $K_1 \in [-4, 2]$ along the forward and backward sweeps, we numerically determine individual phases of each oscillator and a global order parameter to measure the level of synchronisation. Our results reveal how different architectures of simplicial complexes, in conjunction with the interactions and internal-frequency distributions, impact the shape of the hysteresis loop and lead to patterns of locally synchronised groups that hinder global network synchronisation. Remarkably, these groups are differently affected by the size of the shared faces between neighbouring 5-cliques and the presence of higher-order interactions. At $K_1 < 0$, partial synchronisation is much higher in the compact community than in the assemblies of cliques sharing single nodes, at least occasionally. These structures also partially desynchronise at a lower triangle-based coupling K_2 than the compact assembly. Broadening of the internal frequency distribution gradually reduces the synchronisation level in the mixed and sparse communities, even at positive pairwise couplings. The order-parameter fluctuations in these partially synchronised states are quasi-cyclical with higher harmonics, described by multifractal analysis and broad singularity spectra.

I. INTRODUCTION

Mapping complex systems onto networks that embody functional connections among the system's constitutive elements often involves higher-order couplings, which induces more complex geometries. Identifying these hidden geometry features of various orders and assessing their impact on the system's dynamics is currently in the focus of network's theory [1–3] and its applications from the brain [4–6], to large-scale social systems and emergent networks [7–10] to the materials design [11–13]. These complex topologies can be described by algebraic topology [14, 15] with identifying full graphs (cliques) of all sizes that are present as well as the faces that they share with other cliques to make the actual simplicial complex. In this context, the underlying network (1-skeleton of the simplicial complex) is made of the edges connecting two nodes, which may appear as faces of the order one of larger simplexes (triangles, tetrahedrons, etc.).

In the theory of complexity—the emergence of new features at a larger scale, as a key property of a complex system, can be associated with the collective dynamic fluctuations. Such dynamic phenomena, through interactions among dynamical units, appear with long-range spatiotemporal correlations that are characteristics of critical states, either with a dynamical phase transition or as self-organised critical attractors in driven nonlinear dynamics; see a brief survey in [16] and references there. The underlying simplicial struc-

ture can provide multiple interactions among dynamical units associated with the network nodes. Particularly the pairwise interactions occur along the network's edges; meanwhile, the higher interactions can be geometrically embedded into the triangles, tetrahedrons and higher faces up to the largest simplex found in the structure. The two leading (i.e., pairwise and triangle-based) interactions are expected to impact the collective dynamics critically, given the renormalisation-group theory [17, 18]; however, this question remains open in finite systems and complex geometries. The actual impact of these interactions also depends on the type of the dynamics of interacting units. For example, the higher-order interactions, e.g., within large cliques may enable the fast spreading of diseases [19], and enhance traveling waves in networks of neurons but without pathological full synchronised states [20]. On the other side, the triangle-based couplings induce geometric frustration with long-range effects in spin kinetics [21–23].

Phase synchronisation among many interacting units is a prototypical nonlinear dynamics model to study the cooperative phenomena in many complex systems, including applications in neuroscience, engineering, etc. [24–26]. Current research on the influence of higher order coupling on synchronization processes focus on: searching for conditions of perfect synchronization among oscillators on nodes of general networks in the presence of a p -point interactions [27]; conditions for full synchronization between topological signals associated with simplexes of different order; see recent

work [28] and references there; and understanding the nature of synchronisation–desynchronisation processes of the oscillators at nodes of simplicial complexes with geometric interactions embedded into simplexes’ faces of different order [29–33]; Our work belongs to the latter class of problems. In this context, key questions concern the emergence and disappearance of collective dynamic behavior, measured by the order parameter on the hysteresis loop, when the strengths of the various interactions embedded in the geometry vary. For example, the presence of triangle-based interactions is understood to disrupt the order promoted by increasing the strength of pairwise couplings, and can cause sudden desynchronization [29, 32, 34]. Furthermore, the occurrence of *partially synchronised* phases with negative pair interactions is another striking feature of geometric interactions on simplicial complexes; see, for example, [32] and references there. As a special case, the frustrated synchronisation [35] is often attributed to complex structures, e.g., in brain networks, where higher geometries are expected to play an important role [20, 33]. Theoretically, the influence of topology on diffusive processes can be captured to a good extent by spectral analysis of the network [34, 36–39]. A suitable measure is the spectral dimension d_s derived from the eigenvalue spectrum of the Laplace operator associated with the network adjacency matrix; higher-order combinatorial Laplacians [40] are adequate for the diffusion of topological signals on simplicial complexes; see [28]. In the context of phase synchronization, it has been understood that networks with $d_s \geq 4$ are required to enable stable global synchronization, while such states cannot be reached when $d_s \lesssim 2$. Unlike global synchronization, where conditions can be formulated analytically, as in the above references [27, 28], the origin of partial synchronization on simplicial complexes and the nature of the underlying dynamical states are more elusive. In addition to the topological dimension of a simplicial complex, the role of its architecture in synchronization processes remains unclear, especially in relation to by the presence of higher order interactions and the internal inhomogeneity of the nodes’ dynamics.

In this work, we tackle these questions by studying the synchronisation and desynchronisation processes on several 4-dimensional simplicial complexes of a controlled architecture, all assembled by 5-cliques as building blocks [12]. Changing a controlled parameter, as explained in detail in the following section, the assemblies of 5-cliques with different architecture and spectral dimension [38] are grown, which appear to have diverse impacts on phase synchronisation among the oscillators at their nodes. More specifically, we analyse the hysteresis loop by varying the pairwise interaction from negative to positive values and back, with(out) the three-phase couplings embedded into triangles of the actual complex. The network’s ability to reach complete synchrony at the positive pairwise couplings and partial synchrony and incomplete desynchronization by negative interactions depends on the simplicial architecture corroborated with the distribution of internal frequencies. Remarkably, the level of partial synchronisation observed at negative pairwise couplings can be associated with the minimal size of the faces shared among neighbouring 5-cliques and is virtually independent of the presence of higher-

order interactions and the actual frequency distribution. The multifractal fluctuations of the order parameter are associated with these partially synchronised states, emerging through roughly synchronised small clusters. The organisation of clusters is sensitive to the triangle-embedded interactions, even for the global order parameter in the same range.

In section II, we present three considered simplicial complexes and their structural features relevant to this work. Section III introduces the dynamical model with the leading pairwise and triangle-based interactions on these complexes, in III A; then in subsections III B, III C and III D, we give the results regarding the hysteresis properties and individual phases evolution patterns. In sec. IV, we present the multifractal analysis of the order parameter fluctuations in two representative points of the hysteresis loop. Final section V is devoted to a summary and the discussion of the results.

II. STRUCTURE OF THE 5-CLIQUE AGGREGATES WITH DIFFERENT SPECTRAL DIMENSION

To grow the 4-dimensional simplicial complexes for our study, we use the generative model introduced in [12, 41] for a cooperative self-assembly of pre-formatted groups of nanoparticles [11, 42]. As explained in the Introduction, we fix the size of the building blocks as 5-cliques; starting from a single 5-clique, at each growth step, a new clique is attached to the growing structure such that it shares one of its geometrical faces with a clique which is already present in the structure. In the present case, the possible faces are sub-cliques of the size $s = 1, 2, 3$, and 4, respectively, a single node, a link with two adjacent nodes, a triangle with three connected nodes, or a tetrahedron consisting of four nodes. What face would be shared is determined by the geometric compatibility factor and the chemical affinity parameter ν ; see Ref. [12] for a detailed description, and [13] for an extended model with defect cliques. Specifically, the probability of sharing a face of the size s is given by

$$P(s_{max}, s; t) = \frac{c_s(t) e^{-\nu(s_{max}-s)}}{\sum_{s=1}^{s_{max}-1} c_s(t) e^{-\nu(s_{max}-s)}} \quad (1)$$

where $c_s(t)$ stands for the number of geometrically compatible locations on the entire structure at the moment t where docking a simplex of the size s can be done. Note that, in the present case, we have $s_{max} = 5$ fixed. The geometric factor is weighted by the chemical affinity ν [12] towards new $s_{max} - s$ that must be added to the structure after the face with s nodes is shared with a previous clique. Hence, for a large $\nu > 0$, sharing a maximal sub-clique (a tetrahedron) is favoured; the emergent structure is compact. Whereas, when $\nu < 0$, the probability of adding more nodes is increasing. Thus, for a large negative ν , the cliques preferably share a single node (minimal face), resulting in a sparse structure. Without chemical affinity factor, $\nu = 0$, sharing of faces of any size $s = 1, \dots, 4$ can occur, subject to the geometric compatibility factors alone. The resulting structures that we use here are for $\nu = -5$, $\nu = 0$, and $\nu = +5$, shown in Fig. 1.

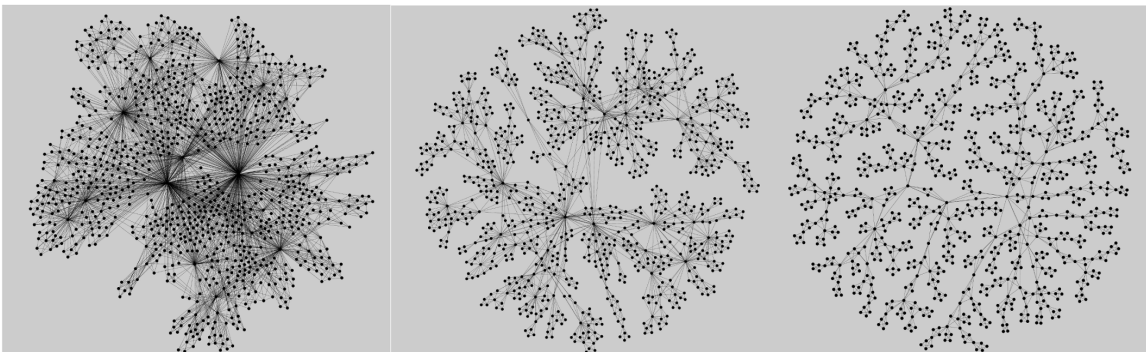


FIG. 1: Networks of 5-cliques grown by the self-assembly rules described in [12] observing the geometric compatibility for different chemical potential, left to right: $v = 5$ (compact), $v = 0$ (mixed), and $v = -5$ (sparse structure). Adding 5-cliques is stopped when the number of nodes reaches $N \geq 1000$.

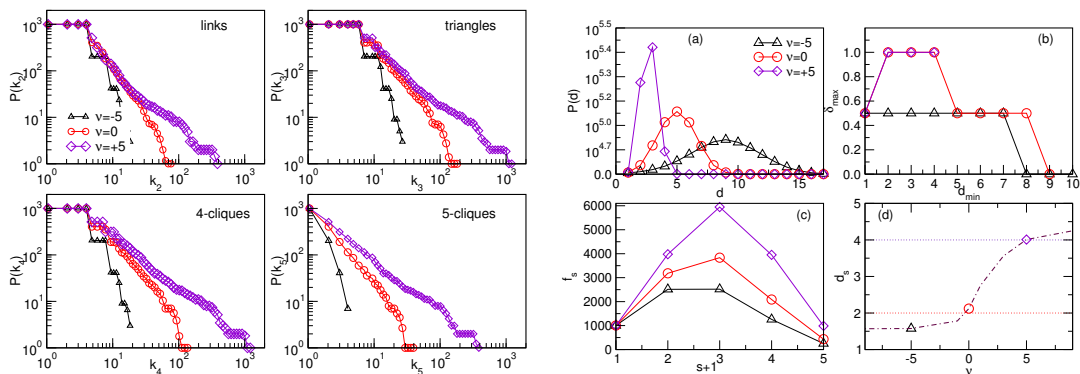


FIG. 2: Left four panels: Cumulative distributions of the generalised degree: the number of edges, triangles, tetrahedra, and 5-cliques per node in three networks for different v , as indicated in the unique legend. Right four panels: (a) The distribution of the shortest-path distances between node pairs, $P(d)$ vs the distance d , (b) the hyperbolicity parameter δ_{max} vs the smallest distance d_{min} of the nodes 4-tuples on these three networks, (c) the number of simplexes f_s of different order q in them, and (d) the network's spectral dimension d_s for different v . The same legend applies to all three panels. The data in panel (d) are from the reference [38].

The structure of these simplicial complexes is characterised by several quantities, cf. Fig. 2, which are relevant to the present study. We determine the generalised-degree distributions $P(k_\mu)$, where k_μ , for $\mu = 2, 3, 4, 5$, indicates the number of edges, triangles, tetrahedra and 5-cliques attached to a node, see Fig. 2 left four panels. The three structures differ significantly in all of these distributions. In particular, the nodes in the compact simplicial complex (at $v = +5$) share a large number of simplexes of all orders, which leads to a distorted power-law distribution at high k_μ ; meanwhile, the distributions of the structure at $v = 0$ with the same number of nodes are nearly power-law with a (finite-size) cut-off). On the other hand, the sparse system, grown with $v = -5$ exhibits a fast decaying exponential distribution for all simplex sizes.

The other measures are compatible with these features, shown in Fig. 2a-d. Specifically, the number of simplexes-and-faces of different sizes that are present in each simplicial structure, f_s , shown in Fig. 2c, indicates that the compact simplicial complex at $v = +5$ possesses the largest number of triangles, and gradually the number of cliques of other sizes, compared to the structure for $v = 0$ and $v = -5$. The underlying network (1-skeleton of these simplicial complexes)

exhibits some other properties that strongly vary with v . In particular, these are the distributions of the shortest-path distances on the underlying graph, shown in Fig. 2a, and the spectral dimension, which is determined for these graphs in ref. [38], shown in Fig. 2d. The spectral dimension for these three representative structures varies, in particular, $d_s = 1.57$, $d_s = 2.11$ and $d_s = 4.01$, for $v = -5$, $v = 0$, and $v = 5$, respectively; they are indicated by different symbols on the line $d_s(v)$, which is determined from the Laplacian eigenvalues distribution in [38] for a range of such structures. Similarly, the distributions on these networks, cf. Fig. 2a, show that small distances prevail in the compact structure for $v = 5$, peaking at $d_{max} = 3$, whereas the peak moves towards larger distances, i.e., $d_{max} = 5$ and $d_{max} = 10$ for $v = 0$ and $v = -5$, respectively. On the other hand, these graphs are 1-hyperbolic by construction; see the discussion in the original work [12]. Specifically, because the cliques (which are $\delta_0 = 0$ -hyperbolic objects) always share their faces in these structures, the hyperbolicity of the emergent complex is given [43, 44] by $\delta_0 + 1$. In Fig. 2b demonstrates it by numerically computing the Gromov hyperbolicity parameter δ_{max} , which does not exceed one considering 10^9 different 4-tuples on these networks.

III. PHASE SYNCHRONISATION ON 4-DIMENSIONAL SIMPLICIAL COMPLEXES

A. Dynamical model and simulations

We consider an ensemble of N coupled Kuramoto oscillators [26] associated with the nodes of a given simplicial complex. The equation governing the evolution of the phase angle θ_i of i^{th} oscillator is given by [32]

$$\begin{aligned} \dot{\theta}_i = & \omega_i + \frac{K_1}{k_i^{(1)}} \sum_{j=1}^N A_{ij} \sin(\theta_j - \theta_i) + \\ & + \frac{K_2}{2k_i^{(2)}} \sum_{j=1}^N \sum_{l=1}^N B_{ijl} \sin(\theta_j + \theta_l - 2\theta_i) \end{aligned} \quad (2)$$

where ω_i 's are the intrinsic frequencies of the phase oscillators. The second and third terms in Eq. (3) represent 1-simplex and 2-simplex interactions, respectively. Note that three-node interactions of the i -th oscillator are based on each 2-simplex (triangle) incident on node i , thus introducing a natural generalization of the pair-wise interaction term [31]. Here, A_{ij} is an element of the 1-simplex adjacency matrix \mathbf{A} , such that $A_{ij} = 1$ if nodes i, j are connected by a link and 0 otherwise. In the second term, B_{ijl} is an element of the 2-simplex adjacency tensor \mathbf{B} , such that $B_{ijl} = 1$ if nodes i, j, l belong to a common 2-simplex (triangle) and 0 otherwise. Likewise, the normalisation factors $k_i^{(1)}$ and $k_i^{(2)}$ indicate the number of links and triangles of the node i , respectively; cf. Fig.2 for the structure of the actual simplicial complexes. The well-known Kuramoto order parameter can effectively quantify the degree of synchronization of the network

$$r = \left\langle \left| \frac{1}{N} \sum_{j=1}^N e^{i\theta_j} \right| \right\rangle, \quad (3)$$

where the brackets $\langle \cdot \rangle$ indicate the time average.

In the simulations, for each network node $i = 1, 2, \dots, N$, where we have $N = 1000, 1002$, and 1003 corresponding to $\nu = 5, 0$, and -5 networks, respectively, the initial conditions for θ_i are chosen randomly in the range $\theta_i \in [0, 2\pi]$. The numerical solution for the set of equations 3 is performed using a numerical integration algorithm ODEINT from Python SciPy library [45]. For each set of parameter values, the system is iterated for 50 000 steps, with the time step $dt = 0.01$ and always considering the previous state of each dynamical variable, the procedure known as tracking the attractor [46] is used in most hysteresis studies. The order parameter in Eq. (3) is calculated in the asymptotic range considering the last 20 000 iterations. Further, to study the hysteresis properties, we track the system's trajectory as the coupling parameter K_1 is first adiabatically increased in steps $dK_1 = 0.1$ in the appropriate range from negative to positive values, typically $K_1 \in [-2, +2]$, constituting the forward sweep, and then decreased along the backward branch. Meanwhile, the strength of the higher-order interaction K_2 kept fixed, and the internal frequencies of the oscillators ω_i are drawn from a given distribution, as explained below.

B. Partial synchronisation at $K_1 < 0$: Hysteresis loop for uniform internal frequencies

In this section, we study hysteresis loop for the interactions embedded in simplexes of different architectures described in sec. II, when the internal frequencies of all oscillators are equal, i.e., $\omega \approx 1.0$ drawn from a δ -function distribution. In this way, we expect that the impact of the structure and related interactions will be more pronounced. As described above in III A, for a given value of K_2 and varying the pairwise coupling strength $K_1 \in [-5, +2]$ in small steps, the order parameter is computed first along the forward branch, and then back. The resulting hysteresis loops for the three networks of Fig. 1, and fixing K_2 to several representatives values between $K_2 = 0.0$ and $K_2 = 1.0$, are summarised in Fig. 3.

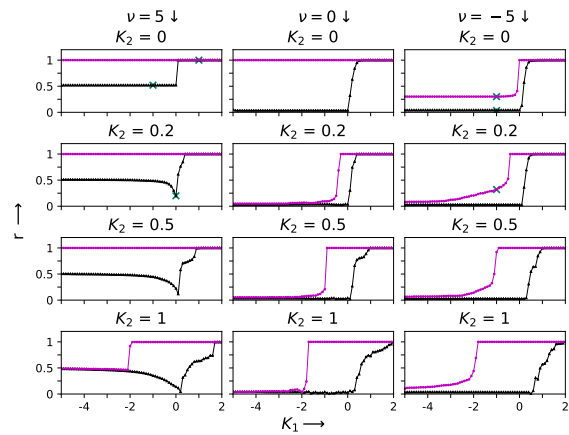


FIG. 3: (Colour online) Hysteresis sweep of the order parameter r as a function of 1-simplex coupling strength K_1 at different 2-simplex coupling strength K_2 ; the three vertical columns (from left to right) correspond to three simplicial complexes in Fig. 1 grown with the chemical affinity $\nu = 5, 0$ & -5 , respectively. In each panel, the solid triangles (black) & solid circles (magenta) refer to forward & backward sweeps, respectively. The intrinsic frequencies $\omega_i \approx 1.0$ at all nodes. The phase evolution patterns analysed in III C correspond to the points indicated by crosses.

As Fig. 3 shows, even though the internal frequencies of the oscillators are equal at all nodes, the shape of the hysteresis loop significantly depends on the structure of the underlying simplicial complexes. On the forward sweep, by keeping $K_2 = 0$, we note the occurrence of partial synchronisation at negative K_1 values, where the order parameter reaches $r \approx 0.5$, for the compact simplicial complex for $\nu = 5$. In the other two networks ($\nu = 0$ and $\nu = -5$), a much smaller but nonzero (within numerical error bars) value $r \approx 0.03$ is observed. Further increasing $K_1 > 0$, a smooth transition to a complete synchronisation with $r \approx 1$ occurs in all networks. On the backward sweep, we note that the synchronised state persists, and the loop does not close even at very large negative K_1 unless the higher-order coupling of a given strength $K_2 > 0$ is applied; moreover, the needed higher-order interaction correlates with the network's compactness. Specifically, in the compact network ($\nu = 5$), cf. lower left panel, the loop

closes for $K_2 = 1.0$ via sudden desynchronisation, in agreement with previous studies [29–32]. However, for $\nu = -5$, an incomplete abrupt desynchronisation occurs even at $K_2 = 0.0$. Still, the loop closes gradually, reaching the forward branch for more negative K_1 values, cf. top right panel and the panels below it. In the intermediate case, $\nu = 0$, a small $K_2 = 0.2$ suffices to induce an incomplete desynchronisation, and the loop gradually closes at more negative K_1 values. By increasing the triangle-based coupling K_2 , the apparent broadening of the loop superimposes these features in each particular network. It is also accompanied by the slower reaching the full synchrony even at high positive pairwise couplings. In the following, we will focus on the evolution of the phases of all oscillators at specific values (K_1, K_2).

C. The dynamics of individual nodes and patterns behind partial synchronisation

The global order parameter r discussed above quantifies the extent to which the oscillators are synchronized at a given set of parameter values. To get a deeper insight into the synchronization and desynchronization processes and their dependence on network geometry and interactions, we study the global phase angle $\theta_{av}(t) = \sum_i \theta_i(t)/N$ as a function of time, the evolution of phase angles of each node, and the distribution of phase angles at a particular time; cf. Fig. 4.

The phase trajectories of individual nodes are shown in the top row of Fig. 4; they are taken at different points marked by crosses on the hysteresis loops in Fig. 3. In particular, these points correspond to the values of the two interactions (K_1, K_2) f, b on the forward f or backward b hysteresis branch are $(-1, 0)f$, $(-1, 0)b$, and $(0, 0.2)f$ for the compact network $\nu = 5$, patterns (a1), (b1) and (c1), respectively. Similarly, the patterns on the panels (d1), (e1) and (f1) correspond to the case $(-1, 0)f$, $(-1, 0)b$, and $(-1, 0.2)b$ for the sparse network with $\nu = -5$. The middle and bottom row below each pattern shows the corresponding network's averaged phase $\theta_{av}(t)$ in the same time interval, and the histogram of phases of individual nodes at the end of that time interval.

For the compact structure ($\nu = 5$), we have that the order parameter $r \approx 0.5$ at the point $(-1, 0)f$; the corresponding pattern of phases, shown in the panel (a1) of Fig. 4, indicates that groups of roughly synchronised nodes are formed and evolve with the same speed. The respective average phase fluctuates in an extended range around π , as shown in panel (a2). In the distribution of nodes' phases, in (a3), broad peaks indicate the formation of three groups of nodes with close but not fully synchronised phases θ_i . The situation is much different at $(-1, 0)b$ in the backward branch, where the system remains fully synchronised, corresponding to a single sharp peak in (b3). The pattern of individual phases in (b1) shows how such a synchronised state forms in time when starting from a random initial state. Consequently, the average phase in (b2) reaches the full range of values on the unit circle. The panels (c1–c3) show how the order parameter appears at the point $(0, 0.2)f$ under the impact of weak triangle-based coupling alone. The pattern in (c1) and the corresponding average

phase in (c2) show that the network's compactness promotes ordering by forming small groups, even though the leading pairwise interaction is absent.

The phase evolution patterns are different in the sparse network ($\nu = -5$), as shown in the panels (d1–f1). At the point $(-1, 0)f$, the order parameter value $r = 0.03$ appears through many small groups of (roughly) synchronised nodes, shown in (d1), corresponding to an almost even distribution of phases over the network nodes, cf. (d3), with tiny fluctuations of the average phase about π , in (d2). At the point $(-1, 0)b$ on the backward branch, the order parameter is dropped from $r = 1$ to a finite value, which is compatible with the pronounced formation of groups visible in the panel (e1) and in the distribution, cf. (e3). The corresponding average phase fluctuates in a larger interval, as shown in the panel (e2). A similar fluctuation range of the average phase is observed in the panel (f2), corresponding to the similar value of the order parameter at the point $(-1, 0.2)b$, cf. Fig. 3. However, the presence of a weak higher-order interaction, in this case, leads to a different grouping of nodes, which is illustrated by the phase evolution pattern in the panel (f1) and the phase histogram in (f3).

D. Hysteresis properties in the transition from uniform to distributed internal frequencies

To explore the impact of the distribution of internal oscillator frequencies, they are drawn from a normal distribution of the width σ centred about $\omega = 1.0$. By increasing the width of the distribution σ , we show that new features of the hysteresis loop appear compared to the case of δ -distribution in Fig. 3, and how these features depend on the network structure. The results for the intermediate width, $\sigma = 0.01$, and a broad distribution $\sigma = 0.1$, are shown in Fig. 5 and Fig. 6, respectively.

Both Fig. 5 and Fig. 6 show that, in the presence of distributed internal frequencies, the partial synchronisation at $K_1 < 0$ persists in all networks with the respective value of the order parameter unchanged compared to the case of δ -distribution, cf. Fig. 3. Moreover, the hysteresis loop is virtually absent unless the higher-order coupling K_2 is switched on. Remarkably lower values of K_2 are needed to induce desynchronisation via an abrupt drop of the order parameter, i.e., in the compact network ($\nu = 5$) compared with the case of homogeneous internal frequencies. We also observe several new features in the forward/backward sweeps. Particularly in the compact network, a drop of the order parameter at $K_1 \leq 0$ occurs before it raises again to reach complete synchrony at $K_1 > 0$; see the left columns in Fig. 5 and Fig. 6. While such a drop is absent in the case of δ -distribution, the area $K_1 \lesssim 0$ where the order parameter is decreasing from the level $r = 0.5$ to zero is broadening with the increasing the frequency distribution width σ . In the sparse and mixed networks, on the other hand, the increasing spread of internal frequencies width σ makes the complete synchronisation increasingly more difficult even at very large $K_1 > 0$. For example, when $\sigma = 0.1$, the pairwise coupling $K_1 \approx 10$ is required for the order parameter to approach $r \lesssim 1$ (not shown). Instead of a steep increase

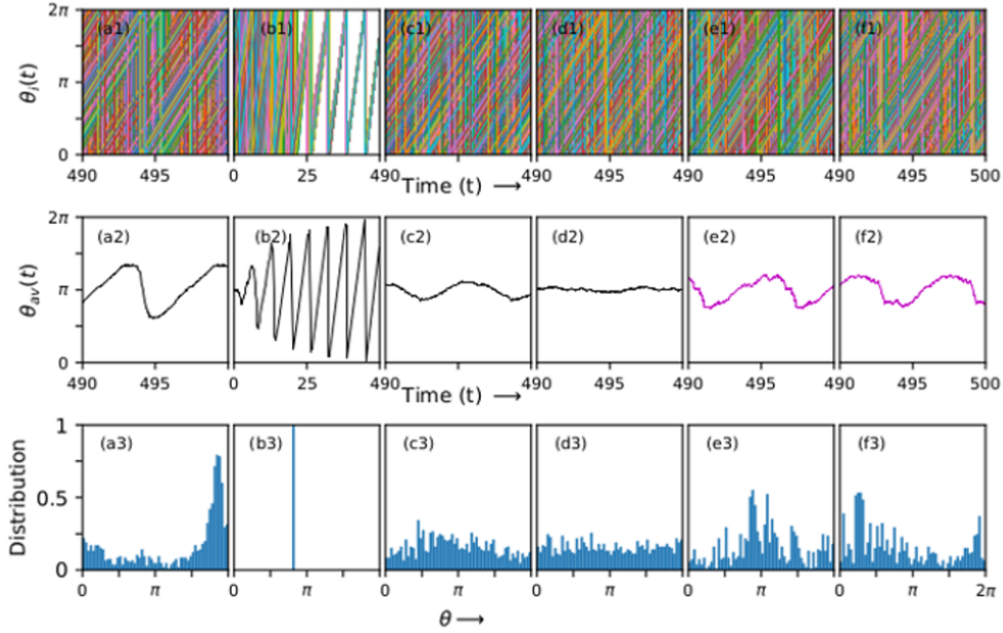


FIG. 4: Colour online) Top row: Individual node's dynamics $\theta_i(t)$ vs time t in the indicated interval (final 1000 time steps, except for the pattern (b1), which is shown for the initial 1000 time steps). The parameter $(K_1, K_2)f, b$ on the forward or backward branch are set as $(-1, 0)f$, $(1, 0)b$, and $(0, 0.2)f$, for the network $\nu = 5$, corresponding to patterns (a1), (b1), and (c1), respectively; meanwhile, the patterns (d1), (e1) and (f1) are for $(-1, 0)f$, $(-1, 0)b$, and $(-1, 0.2)b$ for the sparse network with $\nu = -5$. Middle row: the network averaged phase $\theta_{av}(t)$ as a function of time in the same time interval as the corresponding pattern above it. Bottom row: Histogram of the node's phases θ_i taken at the end of that period corresponding to the panels in the same column above it.

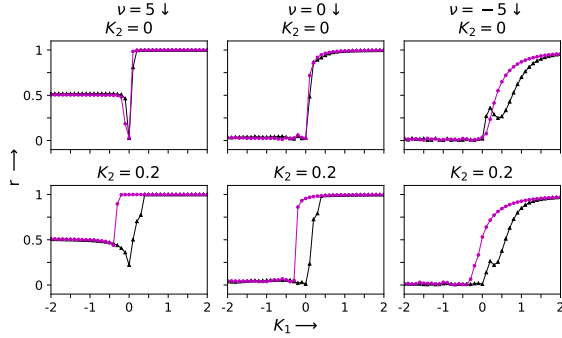


FIG. 5: (Colour online) Transition to synchronization & hysteresis in networks with $\nu = 5, 0, -5$ when, left to right columns, where ω is drawn from a Gaussian distribution width $\sigma = 0.01$ around $\omega = 1.0$; $K_2 = 0$ (top row), and $K_2 = 0.2$ (bottom row). The solid triangles (black) & solid circles (magenta) represent the value of order parameter r in forward & backward sweeps, respectively.

in synchrony for $K_1 \geq 0$, we observe a characteristic instability where the (time-averaged) order parameter achieves different values when the interaction strength K_1 is changed by a small amount; this feature appears both at the forward as well as the backward branch and is practically unaffected by the weak higher-order interactions; see the middle and the right columns in Fig. 6. To a smaller extent, such instability is seen in the sparse network already at a smaller distribution width,

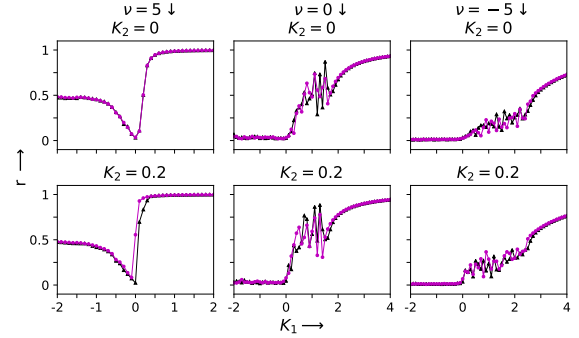


FIG. 6: (Colour online) Same as Fig. 5 but with the ω drawn from a Gaussian distribution with the width $\sigma = 0.1$. In the sparse network, we find that $r \rightarrow 1$ asymptotically at $K_1 \gtrsim 10$ (not shown). Note the absence of hysteresis for these values of higher-order interactions K_2 .

$\sigma = 0.01$, where it causes a kind of hysteresis at the positive K_1 side, as shown in the top right panel of Fig. 5. We note that this feature appears in the networks where the building cliques share a single node, which is 100% in the case of sparse network, and also present in the mixed network, but entirely absent in the compact network; cf. Fig. 1. Understanding the mechanisms of how these instabilities appear is another challenging problem. In the next section, we analyse the nature of the order parameter fluctuations for the values of interactions in the range where the instability occurs in the sparse network.

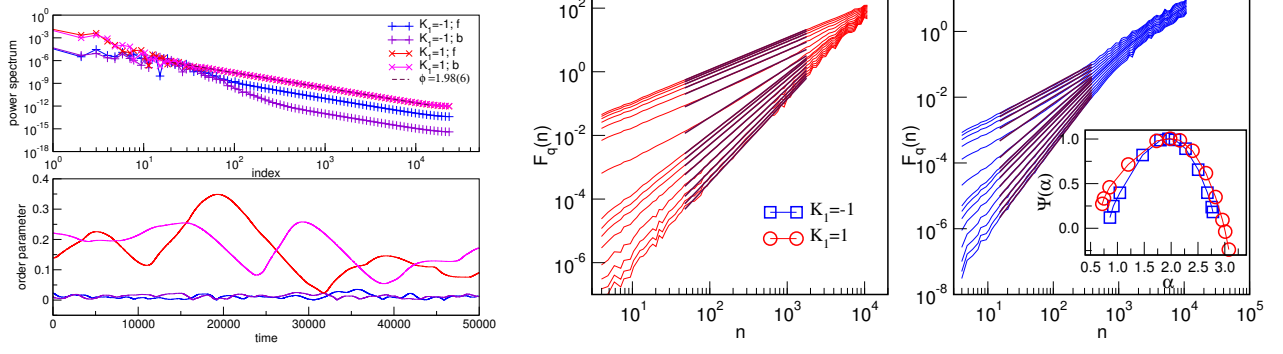


FIG. 7: Left: In the network for $\nu = -5$, the order parameter vs time at two points corresponding to the partial synchronisation at $K_1 = -1$ and $K_1 = 1$ on the forward (f) and backward (b) loop in the absence of higher-order coupling $K_2 = 0$. Middle and right: The fluctuation function $F_q(n)$ vs the time interval n for the order-parameter in the forward loops at $K_1 = -1$ (blue) and $K_1 = 1$ (red). Each line corresponds to different values of the amplification parameter $q \in [-3.5, 3.5]$; the scaling area is indicated by the straight lines giving the generalised Hurst exponent H_q , which leads to the corresponding singularity spectra $\Psi(\alpha)$ vs α given in the inset.

IV. MULTIFRACTAL FLUCTUATIONS OF THE ORDER PARAMETER IN PARTIALLY SYNCHRONISED STATES

In the partially synchronised states in all simplicial complexes, the order parameter for $K_1 < 0$ has finite but different values; the time-averaged values are lower in the sparse networks than the compact ones. Here, we study temporal fluctuations of the order parameter for fixed pairwise interaction strength. Specifically, for the assembly at $\nu = -5$ and a broad Gaussian distribution of the internal frequencies, partial synchronisation occurs at $K_1 < 0$ but also for $K_1 > 0$, reaching a full synchrony asymptotically at very high K_1 ; cf. Fig. 6; we consider two representative points, $K_1 = -1$ and $K_1 = +1$, in the absence of higher-order couplings. The respective time variations of the order parameter, shown in Fig. 7 left panels, both for forward and backward branches of the hysteresis loop exhibit cyclical fluctuations around different average values for $K_1 < 0$ compared to $K_1 > 0$. They lead to the exponent $\phi \sim 2$ compatible with the short-range correlations for an extended portion of the power spectrum at large frequencies; cf. the top left panel in Fig. 7. In the following, we show that these cycles are modulated, attaining higher harmonics, which are captured by the multifractal analysis.

For the analysis of the order parameter fluctuations $r(t)$, we use detrended multifractal analysis of time series [47–49]. Hence, the profile $Y(i) = \sum_{k=1}^i (r(k) - \langle r \rangle)$ of the time series is divided in N_s segments of the length n . Repeating the procedure starting from the end of the time series $t = T_{max}$, we get in total $2N_s = 2 \text{Int}(T_{max}/n)$ segments. Then, at each segment $\mu = 1, 2, \dots, N_s$, the local trend $y_\mu(i)$ is determined, which allows computing the standard deviation around it as $F^2(\mu, n) = \frac{1}{n} \sum_{i=1}^n [Y((\mu - 1)n + i) - y_\mu(i)]^2$, and similarly, $F^2(\mu, n) = \frac{1}{n} \sum_{i=1}^n [Y(N - (\mu - N_s)n + i) - y_\mu(i)]^2$ for $\mu = N_s + 1, \dots, 2N_s$. The fluctuation function $F_q(n)$ for the segment length n is then determined as

$$F_q(n) = \left(\frac{1}{2N_s} \sum_{\mu=1}^{2N_s} [F^2(\mu, n)]^{q/2} \right)^{1/q} \sim n^{H_q}, \quad (4)$$

for different positive and negative values of the amplification parameter q . The function is plotted against varied segment length $n \in [2, \text{int}(T_{max}/4)]$. Its power-law sections on the lines for different q are fitted to find the *generalised Hurst exponent* H_q , defined on the right-hand side of the expression (4). Notably, the case $q = 2$ reduces to the standard deviation function and corresponds to the well-known Hurst exponent.

The spectrum H_q is determined for a range of values of q for which the fluctuation function exhibits scale invariance; here, we use $q \in [-3.5, +3.5]$. Once the spectrum H_q is known, one can determine other multifractality measures, in particular, $\tau_q = qH_q - 1$, where the exponent τ_q , related to the standard (box probability) measure [48]. Then, using the Legendre transform $\Psi(\alpha) = q\alpha - \tau_q$, where $\alpha = d\tau/dq$ the time series *singularity spectrum* can be determined. A nontrivial singularity indicates different power-law singularities at different data points t of the time series, according to $|\nabla r(t, \varepsilon)|_{\varepsilon \rightarrow 0} \sim \varepsilon^{\alpha(t)}$ with an exponent depending on the data point t [47, 48]. Thus, the value $\psi(\alpha)$ stands for a fractal dimension of the time series points having the same singularity exponent α . Note that for a monofractal, $H_q = H_2 = \text{const}$, causing that the spectrum $\Psi(\alpha)$ reduces to a single point $\alpha = H_2$, where H_2 is the standard Hurst exponent.

In Fig. 7, we show the results for the fluctuation function $F_q(n)$ as a function of the time interval n for the order-parameter curves in the forward branch at $K_1 = -1$ (blue) and $K_1 = 1$ (red lines). As these figures show, in both cases, the fluctuation function $F_q(n)$ exhibits a scaling region for a broad range of time intervals n . The fitted area of $F_q(n)$ for different q (indicated by thick dark lines) gives the corresponding H_q exponent defined in eq. (4). In both cases, the resulting broad spectra H_q are transformed onto the singularity spectra $\Psi(\alpha)$, which are given in the inset in the right panel of Fig. 7. The parabolic distribution for both spectra is asymmetrical, having a broad range of values with a maximum close to $\alpha = 2$ and somewhat different curvature. Hence, the mechanisms behind the occurrence of partial synchronisation, as discussed above, are compatible with the multifractal temporal fluctuations of the order parameter with broad singularity spectra.

V. DISCUSSION AND CONCLUSIONS

We have investigated the interplay of structure, interactions and distribution of internal frequencies in phase synchronisation and desynchronisation processes on 4-dimensional simplicial complexes with different architecture composed of identical building blocks (5-cliques); cf. Fig. 1. Of the considered structures, 5-cliques are assembled with rules of chemical affinity and geometric compatibility [12]; when chemical affinity allows the addition of the maximum number of nodes, a minimal face (a node) is shared and a sparse structure appears; oppositely, sharing the largest face (4-clique) leads to a compact assembly. For vanishing chemical affinity, a mixed structure emerges where 5-cliques can share any of their faces by geometric compatibility. The underlying graphs of these simplicial complexes are 1-hyperbolic and have different spectral dimensions [38], as shown in Fig. 2d.

Our results suggest that these simplicial architectures enable geometric frustration effects and diverse collective dynamical phenomena. The shape of the hysteresis loop in the presence of higher-order interactions, as well as the collective fluctuations and the influence of the internal frequency distribution on the synchronisation processes on these simplicial complexes can be related to the size of shared faces by neighbouring 5-cliques. More precisely,

- Partial synchronisation $r < 1$ occurs at negative pairwise coupling with a small non-zero value of the order parameter $r \sim 0.03$ found when the least shared face matches one node ($s = 1$); however, $r \sim 0.5$ when the least common face contains $s = 4$ nodes. Within numerical accuracy, these values of the global order parameter are insensitive to the internal frequency distribution and strength of triangle-based interactions.
- Multiple interactions embedded in triangles change the hysteresis loop and, at a strength that differs for each simplicial complex, induce a sudden drop of the order parameter to the corresponding partial synchronisation level on the negative branch of the pairwise interaction. Moreover, they prolong reaching the full synchronisation with positive pairwise interactions in all simplicial complexes, the effect especially pronounced in the sparse architecture with distributed internal frequen-

cies. Also, in the case of homogeneous frequencies, this structure allows incomplete abrupt desynchronisation even without higher-order coupling.

- The evolution patterns of nodes, analysed at selected points on the hysteresis where partial synchronisation occurs, reveal co-evolving groups with different phases, which leads to quasi-oscillatory fluctuations of the order parameter. These fluctuations have multifractal features with broad singularity spectra associated with the simplicial structure and the interaction strength.

These findings shed new light on the nature of phase synchronisation in high-dimensional simplicial complexes of different architectures in the interplay with coupling strengths and internal frequency distribution. While the transition to synchronisation induced by positive pairwise interactions was much investigated [1], the nature of partial order associated with negative interactions remains to be better understood. In this regard, our simplicial complexes built of identical blocks as 4-dimensional cliques present a potential for studying the complexity of synchronisation/desynchronisation processes in greater detail beyond the measure of the spectral dimension. For example, studying the eigenvector localisation [36] can reveal what mesoscopic structures are involved and the role of node's correlations [32, 33] in the collective dynamics. Moreover, the influence of even/odd numbers of nodes in the shared faces and the geometry-embedded 4th- and 5th-order interactions remain open questions for future study. The results presented here reveal mechanisms behind dynamic states with partial synchronisation, which are often desirable in complex functional systems, e.g., the brain, and ways to construct simplicial complexes of the same order that support full synchronisation when needed.

Acknowledgments

B.T. acknowledge the financial support from the Slovenian Research Agency under the program P1-0044. S.S. acknowledges the financial support from IC&SR, IITM through the project: SB20210838AMMHRD008291. N.G. thanks IC&SR, IITM for the financial support through the project: SP20210777DRMHRDDIRIIT.

-
- [1] S. Boccaletti, P. De Lellis, C.I. del Genio, K. Alfaro-Bittner, R. Criado, S. Jalan, and M. Romance. The structure and dynamics of networks with higher order interactions. *Phys. Reports*, 1018:1–64, 2023.
- [2] M. Boguna, I. Bonamassa, M. De Domenico, S. Havlin, D. Krivoukov and M. Ángeles Serrano. Network geometry. *Nature Review Physics*, 3:114, 2021.
- [3] S. Majhi, M. Perc, and D. Ghosh. Dynamics on higher-order networks: a review. *J. R. Soc. Interface*, 19, 2022.
- [4] A.E. Sizemore, C. Giusti, A. Kahn, and J.M. Vettel. Cliques and cavities in human connectome. *J. Comput. Neurosci.*, 44:115–145, 2018.
- [5] B. Tadić, M. Andjelković, and R. Melnik. Functional geometry of human connectomes. *Sci. Rep.*, 9:12060, 2019.
- [6] M. Andjelković, B. Tadić, and R. Melnik. The topology of higher-order complexes associated with brain hubs in human connectomes. *Sci. Rep.*, 10:17320, 2020.
- [7] M. Andjelković, B. Tadić, S. Maletić, and M. Rajković. Hierarchical sequencing of online social graphs. *Physica A: Statistical Mechanics and its Applications*, 436:582 – 595, 2015.
- [8] B. Tadić, M. Andjelković, B.M. Boshkoska, and Z. Levnajić. Algebraic topology of multi-brain connectivity networks reveals dissimilarity in functional patterns during spoken communications. *PLOS ONE*, 11(11):1–25, 2016.

- [9] M. Andjelković, B. Tadić, M. Mitrović Dankulov, M. Rajković, and R. Melnik. Topology of innovation spaces in the knowledge networks emerging through questions-and-answers. *PLOS ONE*, 11(5):1–17, 2016.
- [10] U. Alvarez-Rodriguez, F. Battiston, G. F. Arruda, Y. Moreno, M. Perc, V. Latora. Evolutionary dynamics of higher-order interactions in social networks. *Nature Human Behaviour*, 5, 2021.
- [11] S. Ikeda and M. Kotani. Materials inspired by mathematics. *Science and Technology of Adv. Materials*, 17(1):253–259, 2016.
- [12] M. Šuvakov, M. Andjelković, and B. Tadić. Hidden geometries in networks arising from cooperative self-assembly. *Sci. Rep.*, 8, 1987, 2018.
- [13] B. Tadić, M. Šuvakov, M. Andjelković, and G. J. Rodgers. Large-scale influence of defect bonds in geometrically constrained self-assembly. *Phys. Rev. E*, 102:032307, 2020.
- [14] D. Kozlov. *Combinatorial Algebraic Topology*. Springer Series Algorithms and Computation in Mathematics, Vol. 21, Springer-Verlag Berlin Heidelberg, 2008.
- [15] J. Johnson. *Some structures and notation of Q-analysis*, volume 8, pages 73–86. 1981.
- [16] B. Tadić and R. Melnik. Self-organised critical dynamics as a key to fundamental features of complexity in physical, biological, and social networks. *Dynamics*, 1(2):181–197, 2021.
- [17] S. Boettcher. Renormalization group for critical phenomena in complex networks. *Frontiers in Physiology*, 2, 2011.
- [18] M. Castellana and G. Parisi. Renormalization group computation of the critical exponents of hierarchical spin glasses. *Phys. Rev. E*, 82:040105, 2010.
- [19] A. Arenas, W. Cota, J. Gómez-Gardeñes, S. Gómez, C. Granell, J.T. Matamalas, et al. Modeling the spatiotemporal epidemic spreading of covid-19 and the Impact of mobility and social distancing interventions. *Phys. Rev. X*, 10:041055, 2020.
- [20] A. Tlaie, I. Leyva, and I. Sendinna-Nadal. Higher-order couplings in geometric complex networks of neurons. *Phys. Rev. Lett.*, 100:052305, 2019.
- [21] Frederic Mila. Frustrated spin systems. *Many-Body Physics: From Kondo to Hubbard*, 5, 2015.
- [22] B. Tadić, M. Andjelković, M. Šuvakov, and G. J. Rodgers. Magnetisation processes in geometrically frustrated spin networks with self-assembled cliques. *Entropy*, 22(3), 2020.
- [23] B. Tadić, N. Gupte. Hidden geometry and dynamics of complex networks: Spin reversal in nanoassemblies with pairwise and triangle-based interactions. *Europhys. Lett.*, 132:60008, 2021.
- [24] J. Fell, N. Axmacher. The role of phase synchronization in memory processes. *Nature Rev. Neurosci.*, 12:105–118, 2011.
- [25] L. Gollo and Breakspear M. The frustrated brain: from dynamics on motifs to communities and networks. *Phil. Trans. R. Soc. B*, 2014.
- [26] F.A. Rodrigues, T. Peron, P. Ji, and J. Kurths. The kuramoto model in complex networks. *Physics Reports*, 610:1–98, 2016.
- [27] S. Dutta, P. Kundu, P. Khanra, C. Hens, and P. Pal. Perfect synchronization in complex networks with higher order interactions. *arxiv:physics*, 2303.09213, 2023.
- [28] T. Carletti, L. Giambagli, and G. Bianconi. Global topological synchronization on simplicial and cell complexes. *Phys. Rev. Lett.*, 130:187401, 2023.
- [29] P. S. Skardal and A. Arenas. Higher order interactions in complex networks of phase oscillators promote abrupt synchronization switching. *Commun. Physics*, 3(1), 2020.
- [30] R. Ghorbanchian, J. Restrepo, J.J. Torres, and G. Bianconi. Higher-order simplicial synchronization of coupled topological signals. *arXiv:2011.00897v1*, 2020.
- [31] K. Kovalenko et al. Growing scale-free simplices. *Communications physics*, 4:43, 2021.
- [32] M. Chutani, B. Tadić, and N. Gupte. Hysteresis and synchronization processes of kuramoto oscillators on high-dimensional simplicial complexes with competing simplex-encoded couplings. *Phys. Rev. E*, 104:034206, 2021.
- [33] B. Tadić, M. Chutani, and N. Gupte. Multiscale fractality in partial phase synchronisation on simplicial complexes around brain hubs. *Chaos, Solitons & Fractals*, 160:112201, 2022.
- [34] A.P. Millán, J.J. Torres, and G. Bianconi. Synchronization in network geometries with finite spectral dimension. *Physical Review E*, 99(2):022307, 2019.
- [35] M. Khoshkhou and A. Montakhab. Explosive, continuous and frustrated synchronization transition in spiking hodgkin–huxley neural networks: The role of topology and synaptic interaction. *Physica D: Nonlinear Phenomena*, 405:132399, 2020.
- [36] M. Mitrović and B. Tadić. Spectral and dynamical properties in classes of sparse networks with mesoscopic inhomogeneities. *Phys. Rev. E*, 80:026123, 2009.
- [37] C. Castellano and R. Pastor-Satorras. Relating topological determinants of complex networks to their spectral properties: Structural and dynamical effects. *Phys. Rev. X*, 7:041024, 2017.
- [38] M. Mitrović Dankulov, B. Tadić, and R. Melnik. Spectral properties of hyperbolic networks with tunable aggregation of simplices. *Physical Review E*, 100:012309, 2019.
- [39] A.P. Milan, J.J. Torres, and G. Bianconi. Complex network geometry and frustrated synchronization. *Sci. Rep.*, 8, 2018.
- [40] D. Horak and J. Jost. Spectra of combinatorial laplace operators on simplicial complexes. *Adv. Math.*, page 303, 2013.
- [41] M. Šuvakov, M. Andjelković, and B. Tadić. Applet: Simplex aggregated growing graph (<http://suki.ipb.rs/ggraph/>). 2017.
- [42] S. Samaresh, P. Raval, R. G.N. Manjurata, and C. Debangshu. Cooperative self-assembly driven by multiple noncovalent interactions: Investigating molecular origin and reassessing characterization. *ACS Cent. Sci.*, 7(8), 2021.
- [43] S. Bermudo, J. M. Rodríguez, J. M. Sigarreta, and J.-M. Vialaire. Gromov hyperbolic graphs. *Discrete Mathematics*, 313(15):1575 – 1585, 2013.
- [44] N. Cohen, D. Coudert, G. Ducoffe, and A. Lancin. Applying clique-decomposition for computing gromov hyperbolicity. *Theoretical Computer Sci.*, 690(Suppl. C):114 – 139, 2017.
- [45] P. Virtanen, R. Gommers, T.E. Oliphant, M. Haberland, T. Reddy, et al. *SciPy 1.0: Fundamental algorithms for scientific computing in python*. *Nat. Methods*, 2020.
- [46] A. Roy and N. Gupte. The transition to synchronization on branching hierarchical lattices. *em Chaos*, 32, 013120, 2022.
- [47] A.N. Pavlov and V.S. Anishchenko. Multifractal analysis of complex signals. *Physics–Uspekhi*, 50:819–834, 2007.
- [48] J.W. Kantelhardt et al. Multifractal detrended fluctuation analysis of nonstationary time series. *Physica A: Statistical Mechanics and its Applications*, 316:87–114, 2002.
- [49] B. Tadić. Multifractal analysis of Barkhausen noise reveals the dynamic nature of criticality at hysteresis loop. *J. Statistical Mechanics: Theory and Experiment*, 6:063305, 2016.